Interfaces and Free Boundaries **18** (2016), 91–113
DOI 10.4171/IFB/358

Effective behavior of an interface propagating through a periodic elastic medium

PATRICK W. DONDL
Abteilung für Angewandte Mathematik, Albert-Ludwigs-Universität Freiburg, Hermann-Herder-Str. 10, 79104 Freiburg i. Br., Germany
E-mail: patrick.dondl@mathematik.uni-freiburg.de

KAUSHIK BHATTACHARYA
Mail Stop 104-44, California Institute of Technology, Pasadena, CA 91125, USA
E-mail: bhatta@caltech.edu

[Received 20 February 2015 and in revised form 29 June 2015]

We consider a moving interface that is coupled to an elliptic equation in a heterogeneous medium. The problem is motivated by the study of displacive solid-solid phase transformations. We argue that a nearly flat interface is given by the graph of the function g which evolves according to the equation $g_t(x) = -(-\Delta)^{1/2}g(x) + \varphi(x, g(x)) + F$ where $-(-\Delta)^{1/2}g$ describes the elasticity of the interface, $\varphi(x, g(x))$ the heterogeneity of the media and F the external force driving the interface. This equation also arises in the study of ferroelectric and ferromagnetic domain walls, dislocations, fracture, peeling of adhesive tape and various other physical phenomena. We show in the periodic setting that such interfaces exhibit a stick-slip behavior associated with pinning and depinning. Specifically, there is a critical force $F^\star$ below which the interface is trapped, and beyond which the interface propagates with a well-described effective velocity that depends on F. We present numerical evidence that the effective velocity ranges from $v \sim (-\log|F - F^\star|)^{-1}$ to $(F - F^\star)^\beta$ for some $0 < \beta \leqslant 1$ for F close to $F^\star$ depending on φ. We obtain $\beta = 1/2$ for the case of non-degenerate smooth obstacles. We further present numerical evidence that $F^\star$ can depend on direction and sense of propagation.

2010 Mathematics Subject Classification: Primary 35B27; Secondary 35R35.

Keywords: Fractional Laplacian, interfaces, heterogeneous media, effective properties, homogenization, periodic media, free boundary problems, pinning.

1. Introduction

Hysteresis is ubiquitous in materials science, and is associated with nucleation and propagation of interfaces and defects. This paper concerns the propagation of interfaces immersed in an elastic medium. The paper is specifically motivated by phase boundaries in solids that undergo a displacive phase transformation such as the martensitic phase transformation. Similar equations also arise in the study of ferroelectric and ferromagnetic domain walls, dislocations, fracture, peeling of adhesive tape and various other physical phenomena.

In displacive phase transformations, one has phase boundaries across which the crystal structure changes without any diffusion or loss of compatibility. Many interesting properties of such materials, like the shape-memory effect, are associated with the nucleation and evolution of these phase boundaries. As the interface propagates, the change in crystal structure potentially gives rise

to elastic fields. Thus, one has a moving interface problem that is coupled to an elasticity problem. Further, every material contains defects like non-transforming precipitates which make the medium inhomogeneous. These defects affect the state of stress, and thus the propagation of the phase boundary. An understanding of the role of defects on interface propagation motivates the current work.

There is a well-developed framework to study the evolution of martensitic phase boundaries, and this is described in detail in the monograph of Abeyaratne and Knowles [3]. Briefly, one defines a thermodynamic driving force either through the rate of dissipation or through the variation in the total energy with respect to the position of the interface, and then postulates a kinetic relation that relates the driving force to the normal velocity of the interface. Microscopic theories suggest that the kinetic relation has viscous character passing smoothly through the origin [2, 22]. Such a kinetic relation predicts that the hysteresis goes to zero as the rate of loading goes to zero. However, experiments clearly show otherwise: the hysteresis does not go to zero with loading rate and instead settles on a non-zero value independent of loading-rate for slow enough rates. Such observations suggest a stick-slip behavior where the interface is stationary below a critical driving force and moves freely above it. It is often suggested that pinning of the phase boundary by defects is responsible for this transition from microscopic viscous to macroscopic stick-slip behavior.

A one-dimensional calculation, as found in [1, 5, 19] illustrates how a local wiggly potential can pin a phase boundary and lead from a linear kinetic relation to a stick-slip behavior. Assume a bar with a 1-periodic local driving force $\varphi(x)$ (smooth and with non-degenerate global maximum and minimum), and assume that the velocity of the interface is given as $v = F + \varphi(x)$, where F is the constant external applied force and $-\varphi(x)$ is a local material back-stress impeding propagation. The amount of time it takes for the interface to travel one period can now easily be calculated to be

$$T = \int_0^1 \frac{\mathrm{d}g}{F + \varphi(g)}, \tag{1}$$

if $F > -\min\varphi$ or $F < -\max\varphi$. Otherwise (i.e., if $-\min\varphi \geqslant F \geqslant -\max\varphi$), the time is infinite and the interface is stuck. Further, close to the critical F, say $F \approx -\max\varphi$, the interface is slow only in a few isolated points but propagates freely elsewhere. This implies, under some non-degeneracy and regularity conditions, that the effective velocity scales as the square-root of the excess force. Thus, the effective velocity $\bar{v} = \frac{1}{T}$ of the interface now exhibits a behavior of the form shown in Figure 1. The question whether such a stick-slip behavior is also observed in models for phase transformations in higher dimension motivates this work.

We present a sharp interface model for the quasistatic evolution of a martensitic phase boundary in higher dimensions in Section 2. We limit ourselves to the scalar setting where the displacements are scalars (anti-plane shear in two dimensions) though the ideas and results hold for the general case. In this model, a free boundary separates two material phases. Each phase is characterized by a distinct transformation or stress-free strain where the elastic energy density admits its minimum. We also assume that the material contains a number of non-transforming precipitates. Importantly, we assume that both the phases as well as the non-transforming precipitates have the same elastic moduli. A similar model was studied by Craciun [6].

We then derive an approximate model for a nearly flat interface. We show, using methods of Γ-convergence, that the elastic energy of a nearly flat interface is approximated by the $H^{1/2}$-norm of a function whose graph describes the interface (Theorem 2.1). We also argue that at low volume fraction, the precipitates give rise to a local forcing which scales similarly to the elastic energy. We

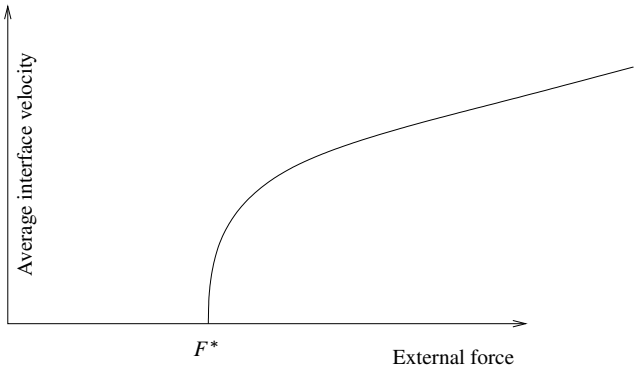

FIG. 1. Pinning-depinning behavior as calculated from a one-dimensional model in [5]. The interface is stuck up to a critical force F^*, and breaks free above it with a particular scaling. For large F, the average velocity is linear in the applied force.

thus conclude that the interface is described by the graph of a function g which is governed by the equation

$$g_t = -(-\Delta)^{1/2} g + \varphi\big(x_1, \ldots, x_n, g(x_1, \ldots, x_n)\big) + F \tag{2}$$

for a given $\varphi : \mathbb{R}^{n+1} \to \mathbb{R}$ with zero mean. In two dimensions, it can be written using an integral representation

$$g_t(x,t) = c \int \frac{g(x',t)}{|x-x'|}\, \mathrm{d}x' + \varphi(x,t) + F. \tag{3}$$

On the periodic domain we consider, this equation may be compactly written by its Fourier series,

$$\hat{g}_t(k,t) = -|k|\, \hat{g}(k,t) + \widehat{\varphi(x, g(x,t))}(k) + \hat{F}. \tag{4}$$

From now on, $\hat{g}$ indicates the Fourier series of the periodic function g. Note that the equation is still nonlinear, since the driving force φ depends on g.

While we derive this model from phase transformations in the scalar shear setting, the same model with some different coefficients hold in the vectorial setting when the two stress-free strains are kinematically compatible. The model (2) has also been used to study dislocations [13, 14, 18, 20], fracture [15, 21, 23], peeling of adhesive film [25, 26] in the presence of heterogeneities. Similar models can be derived for ferroelectric and ferromagnetic domains.

A closely related parabolic model,

$$g_t = \Delta g + \varphi + F \tag{5}$$

has been used to study pinning of surface energy dominant interfaces by defects. The large physics literature has concentrated on the situation where φ is random, and has shown using scaling arguments and numerical simulation that these equations lead to a pinning/depinning transition with a critical exponent which varies from situation to situation [4]. Dirr and Yip [9] presented a rigorous analysis of the parabolic model (5) in the periodic setting (φ is periodic). A rigorous analysis of the random case remains the topic of ongoing research (see for example [7, 8]).

We study the behavior of the solutions of (2) in Section 3 where φ is (1−)periodic. We show that there is a critical $F^* \geqslant 0$ such that (2) admits a stationary solution for all $F \leqslant F^*$ (Theorem

3.5). Further, for each $F > F^*$, there exists an unique T such that (2) admits a space-time periodic solution (Theorem 3.7 and Proposition 3.9). Thus, we may regard $1/T$ as the effective velocity of the interface. These results are similar to those obtained by Dirr and Yip [9] for the parabolic equation, and our methods closely follow theirs.

In Section 4, we discuss the behavior of the effective velocity near the depinning transition. We show that wide range of behavior is possible depending on the nature of φ at the critical pinning state. Specifically, the effective velocity can range from $v \sim (-\log|F - F^\star|)^{-1}$ to $(F - F^\star)^\beta$ for some $0 < \beta \leqslant 1$ for F close to $F^\star$ depending on φ. We obtain the logarithmic behavior if the obstacles are sharp near the critical state while we obtain $(F - F^\star)^1$ for those that are flat. We obtain $v \sim (F - F^\star)^{1/2}$ for non-degenerate smooth obstacles.

2. A model of phase transformations

2.1 *Phase transformations in the presence of defects*

We consider a model proposed by Craciun [6]. Since we are interested in the overall propagation, we consider the domain to be a strip, $\Omega = T^n \times \mathbb{R}$ where T^n is an n-dimensional torus as shown in Figure 2. The domain Ω is divided into two parts, E and $\Omega \setminus E$ occupied by two phases, and separated by the phase boundary Γ of codimension 1. The domain also contains a number of non-transforming precipitates, occupying the set $\bigcup_i A_i$. The two phases are characterized by two stress-free strains $\xi^\pm \in \mathbb{R}^{n+1}$, and the non-transforming precipitates are characterized by the stress-free strain ξ^0. We further assume that all phases and precipitates have equal elastic modulus (which we take to be identity without loss of generality). Thus the elastic energy of domain subjected to the

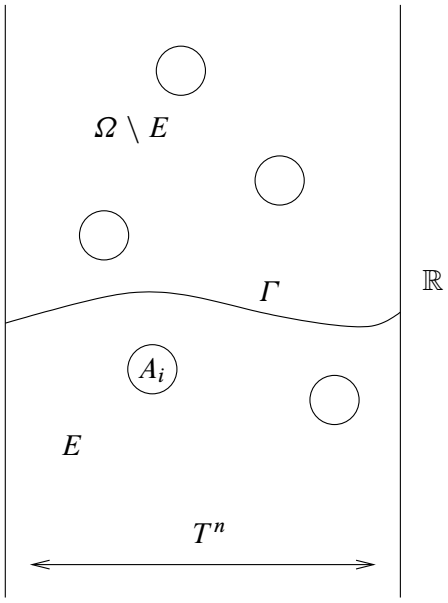

FIG. 2. A phase boundary in a strip containing non-transforming precipitates

displacement $u : \Omega \to \mathbb{R}$ is given by

$$\mathcal{F}_{\text{elastic}} = \int_{\Omega} \frac{1}{2} ||\nabla u - \xi_E||^2 \, \mathrm{d}x\mathrm{d}y. \tag{6}$$

where

$$\xi_E(x, y) = \begin{cases} \xi^+ & (x, y) \in E \setminus \bigcup_i A_i, \\ \xi^- & (x, y) \in (\Omega \setminus E) \setminus \bigcup_i A_i, \\ \xi^0 & (x, y) \in \bigcup_i A_i. \end{cases} \tag{7}$$

and ∇ denotes gradient with respect to (x, y) for $x \in T^n$, $y \in \mathbb{R}$.

For a given interface Γ, we obtain the displacement by minimizing the energy subject to appropriate boundary conditions. This displacement satisfies the Euler-Lagrange equation

$$\Delta u = \operatorname{div} \xi_E. \tag{8}$$

We then say that the interface Γ evolves in a specified manner that reduces the (optimal) elastic energy [3].

Due to the linearity of the Euler-Lagrange equation (8), one can split the transformation strain and the displacement into components depending only on the interface and on the precipitates, respectively. Take

$$u = u_\Gamma + u_P; \quad \xi_E = \xi_\Gamma + \xi_P \tag{9}$$

and fix

$$\xi_\Gamma(x) = \begin{cases} \xi^+ & x \in E, \\ \xi^- & x \in (\Omega \setminus E), \end{cases} \tag{10}$$

and

$$\xi_P(x) = \begin{cases} \xi^0 - \xi^+ & x \in \bigcup_i A_i \cap E, \\ \xi^0 - \xi^- & x \in \bigcup_i A_i \cap (\Omega \setminus E). \end{cases} \tag{11}$$

The displacements u_P, u_Γ solve the Euler-Lagrange equations associated with ξ_Γ, ξ_P,

$$\Delta u_\Gamma = \operatorname{div} \xi_\Gamma; \quad \Delta u_P = \operatorname{div} \xi_P. \tag{12}$$

This fixes the functions u_Γ and u_P up to an affine component.

Substituting this decomposition back into the elastic energy, we can expand it as follows:

$$\begin{aligned} \int_{\Omega} \frac{1}{2} ||\nabla u - \xi_E||^2 \, \mathrm{d}x\mathrm{d}y = \int_{\Omega} \frac{1}{2} ||\nabla u_\Gamma - \xi_\Gamma||^2 \, \mathrm{d}x\mathrm{d}y \\ + \int_{\Omega} (\nabla u_P - \xi_P) \cdot \nabla u_\Gamma \, \mathrm{d}x\mathrm{d}y \\ - \int_{\Omega} (\nabla u_P - \xi_P) \cdot \xi_\Gamma \, \mathrm{d}x\mathrm{d}y \\ + \int_{\Omega} \frac{1}{2} ||\nabla u_P - \xi_P||^2 \, \mathrm{d}x\mathrm{d}y \end{aligned} \tag{13}$$

The first term in (13) is the energy associated with the interface Γ in the absence of any precipitates. We shall call this the *self-energy* of the interface and denote it by $\mathcal{F}_{\text{self}}$. Integrating by parts once and using the Euler-Lagrange equation (12), the second term becomes a boundary integral. Assuming

that $\nabla u_P - \xi_P$ remains finite, this term vanishes as long as u_Γ vanishes as $y \to \pm\infty$. Given a smooth interface Γ and using the freedom of adding a piecewise affine function as below, such a choice of u_Γ is possible. The last two terms describes the interaction of the precipitates with the interface, and we denote it $\mathcal{F}_{\text{int}}$.

2.2 *Small volume fraction of precipitates*

We seek to find an approximation for this particular model when the volume fraction of precipitates is small and the phase boundary is disjoint from the precipitates. To motivate the approximation, consider the situation where one does not have any non-transforming precipitates and the interface that minimizes the total energy. It is easy to show in the current scalar setting that the interface is a plane with normal $n = (\xi^+ - \xi^-)/|\xi^+ - \xi^-|$[1]. Therefore, we expect that an arbitrary interface will soon become almost planar with this normal and then evolve in an almost planar manner. Further, in the presence of defects, we expect the interface to be distorted close to them due to the elastic fields created by the defects but be largely planar away from them. Thus, if the concentration of defects is small, the interface remains largely planar. This is consistent with numerical observations [10]. All of this motivates us to seek an approximation for the model in the case that the interface is almost planar. We find a rigorous approximation for the self energy in Section 2.3, and a heuristic one for the interaction energy in Section 2.4. The final approximate model is described in Section 2.5.

By a change of variables, we obtain the special case

$$\xi^{\pm} = (0, \ldots, 0, \pm 1/2)^{\mathrm{T}} \tag{14}$$

and the preferred normal is $n = (0, \ldots, 0, 1)^T$ without any loss of generality. We assume that the phase boundary is the graph of a H^1 and essentially bounded function g, i.e.,

$$\Gamma = \big\{(x_1, x_2, \ldots, x_n, y) \text{ such that } y = g(x_1, \ldots, x_n)\big\}, \tag{15}$$

and the transformed domain $E = \{(x, y) : y < g(x)\}$.

Now, let us assume that the precipitates occupy a small volume fraction ε:

$$A_i^\varepsilon = (x_i^\varepsilon, y_i^\varepsilon) + \varepsilon^{1/n} A_i, \tag{16}$$

where $x_i^\varepsilon, y_i^\varepsilon$ are chosen such that the barycenter of each obstacle remains fixed under the rescaling. It is easy to show that the resulting elastic displacements u_P^ε that solve (12) scales as $u_P^\varepsilon = \varepsilon U_P$. Therefore, we seek a scaling for the interface so that the corresponding displacements u_Γ^ε has the same scaling. This motives the following scaling for the interface:

$$\Gamma^\varepsilon = \big\{(x, y) = y_0 + \varepsilon g\big\}. \tag{17}$$

We assume that $y_0 \neq y_i$ for any i so that the interface is disjoint from the precipitates for small enough ε.

We now see that

$$\mathcal{F}^\varepsilon_{\text{elastic}} = \varepsilon^2 \int_\Omega \frac{1}{2} \left|\left|\nabla U - \xi_E^\varepsilon\right|\right|^2 \mathrm{d}x\mathrm{d}y \tag{18}$$

[1] In the vectorial setting of linearized elasticity, there are two possible normals [17]. We can proceed with either of these.

where

$$\xi_E^\varepsilon(x,y) = \begin{cases} \frac{1}{\varepsilon}\xi^+ & (x,y) \in E^\varepsilon \setminus \bigcup_i A_i^\varepsilon, \\ \frac{1}{\varepsilon}\xi^- & (x,y) \in (\Omega \setminus E^\varepsilon) \setminus \bigcup_i A_i^\varepsilon, \\ \frac{1}{\varepsilon}\xi^0 & (x,y) \in \bigcup_i A_i^\varepsilon. \end{cases} \tag{19}$$

Therefore, we seek approximations to $\frac{1}{\varepsilon^2}\mathcal{F}_{\text{self}}$ and $\frac{1}{\varepsilon^2}\mathcal{F}_{\text{int}}$.

In order to do so, it is convenient to subtract the piecewise constant, curl-free, function $\frac{1}{2}(y_0 - H(y))$[2] from the transformation strain ξ_E^ε, in order to make it supported in a bounded region around $y = 0$. This does not change the energy of minimizers of the energy functional, since one can simply subtract the respective integral from u. From now on, we thus assume that, for a given function $\tilde{g}\colon T^n \to \mathbb{R}$,

$$\xi_{\tilde{g}}^n(x,y) = \begin{cases} 0 & \text{for } y \leqslant y_0 \text{ and } y \leqslant \tilde{g}, \\ -1 & \text{for } y \leqslant y_0 \text{ and } y > \tilde{g}, \\ 1 & \text{for } y > y_0 \text{ and } y \leqslant \tilde{g}, \\ 0 & \text{for } y > y_0 \text{ and } y > \tilde{g} \end{cases} \tag{20}$$

and $\xi_{\tilde{g}}(x,y) = \begin{pmatrix} 0 \\ \vdots \\ 0 \\ \xi_{\tilde{g}}^n(x,y) \end{pmatrix}$. With this change, the scaled self energy of the interface is the minimum of the functional

$$\mathcal{F}_\varepsilon(u) = \int_\Omega \frac{1}{2} \left|\left| \nabla u - \frac{1}{\varepsilon}\xi_{\varepsilon g} \right|\right|^2, \tag{21}$$

while the scaled interaction energy is

$$\mathcal{F}_{\text{int}}^\varepsilon = -\int_{E\setminus\{y\leqslant y_0\}} (\nabla u_P - \xi_P)\cdot\xi_\Gamma \mathrm{d}x\mathrm{d}y + \int_{\{y\leqslant y_0\}} (\nabla u_P - \xi_P)\cdot\xi_\Gamma \mathrm{d}x\mathrm{d}y + \int_\Omega \frac{1}{2}\left|\left| \nabla u_P - \frac{1}{\varepsilon}\xi_{\varepsilon^{1/n}P} \right|\right|^2 \mathrm{d}x\mathrm{d}y \tag{22}$$

2.3 *Approximation of the self-energy*

Let $g \in H^1(T^n) \cap L^\infty(T^n)$. Consider the scaled self energy functional

$$\mathcal{F}_\varepsilon(u) = \int_\Omega \frac{1}{2} \left|\left| \nabla u - \frac{1}{\varepsilon}\xi_{\varepsilon g} \right|\right|^2, \tag{23}$$

for ε small. We show that this functional converges in the sense of Γ-convergence with respect to the usual L^1_{loc} metric, to the limit functional

$$\mathcal{F}(u) = \begin{cases} \int_{\Omega\setminus\{y=0\}} \frac{1}{2}\,||\nabla u||^2 & \text{if } [\![u]\!] = g \text{ a.e.} \\ \infty & \text{otherwise.} \end{cases} \tag{24}$$

[2] $H(y)$ denotes the Heaviside step function.

Both functionals are assumed to be infinite if $u \notin H^1_{\text{loc}}$. The expression $[\![u]\!]$ denotes the jump of u across $\{y = 0\}$ (i.e., the difference of the respective traces). We write

$$u^+_\varepsilon(x, y) = u_\varepsilon(x, y + \varepsilon),$$
$$u^-_\varepsilon(x, y) = u_\varepsilon(x, -y - \varepsilon).$$

Without loss of generality, we assume here that $||g||_{L^\infty} \leqslant 1$, otherwise the definition of $u^\pm_\varepsilon(x, y)$ needs to be adapted so that the interface does not penetrate outside the cutout region.

Theorem 2.1 (Approximation of the energy) *Let $(\varepsilon_j)_{j\in\mathbb{N}}$ be a decreasing sequence of positive real numbers converging to zero. The following assertions hold.*

(i) *Consider functions u_{ε_j} such that $\mathcal{F}_{\varepsilon_j}(u_{\varepsilon_j})$ is uniformly bounded. Then there exists a subsequence (which we relabel and also index by j) and functions $u^\pm \in H^1_{\text{loc}}(T^n \times (0, \infty))$, such that*

$$u^+_{\varepsilon_j} \rightharpoonup u^+,$$
$$u^-_{\varepsilon_j} \rightharpoonup u^-$$

weakly in $H^1_{\text{loc}}(T^n \times (0, \infty))$ (and thus strongly in L^1_{loc}), modulo a constant function.

(ii) *Given a sequence u_{ε_j}, such that $u^\pm_{\varepsilon_j} \to u^\pm$ in $L^1_{\text{loc}}(T^n \times (0, \infty))$, we have*

$$\liminf \mathcal{F}_{\varepsilon_j}(u_{\varepsilon_j}) \geqslant \mathcal{F}(u), \tag{25}$$

where $u(x, y) = u^\pm(x, \pm y)$ for $y > 0$ (+) or $y < 0$ (−), respectively.

(iii) *Given $u \in H^1(\Omega\backslash\{y = 0\})$, there exists a sequence u_{ε_j} so that $u^+_{\varepsilon_j} \to u$ in $L^1_{\text{loc}}(T^n\times(0, \infty))$, $u^-_{\varepsilon_j} \to u(x, -y)$ in $L^1_{\text{loc}}(T^n \times (0, \infty))$, and*

$$\limsup \mathcal{F}_{\varepsilon_j}(u_{\varepsilon_j}) \leqslant \mathcal{F}(u). \tag{26}$$

Proof. (i) Clearly, $\int_{T^n\times(0,\infty)} \left|\left|\nabla u^\pm_\epsilon\right|\right|^2$ is uniformly bounded. This yields the desired compactness.

(ii) If $[\![u]\!] = g$, the result is immediate from the definition of the energies. What remains to show, is that the elastic energy necessarily blows up if the difference of the respective traces of $u_\varepsilon(x, \varepsilon)$ and $u_\varepsilon(x, -\varepsilon)$ does not converge to the function g. Note that, for all ε, one can calculate

$$\begin{aligned}
\mathcal{F}_\varepsilon(u_\varepsilon) &\geqslant \int_{T^n}\int_{-\varepsilon}^{\varepsilon} \frac{1}{2}\left|\left|\nabla u_\varepsilon - \frac{1}{\varepsilon}\xi_{\varepsilon g}\right|\right|^2 \\
&\geqslant \int_{T^n}\int_{-\varepsilon}^{\varepsilon} \frac{1}{2}\left|\frac{\partial}{\partial y}u_\varepsilon - \frac{1}{\varepsilon}H\big(\varepsilon g(x) - y\big) + \frac{1}{\varepsilon}H(-y)\right|^2 \\
&\geqslant \frac{1}{2\varepsilon}\int_{T^n}\frac{1}{2}\left(\int_{-\varepsilon}^{\varepsilon}\left|\frac{\partial}{\partial y}u_\varepsilon - \frac{1}{\varepsilon}H\big(\varepsilon g(x) - y\big) + \frac{1}{\varepsilon}H(-y)\right|\right)^2 \qquad (27) \\
&\geqslant \frac{1}{2\varepsilon}\int_{T^n}\frac{1}{2}\left|\int_{-\varepsilon}^{\varepsilon}\frac{\partial}{\partial y}u_\varepsilon - \frac{1}{\varepsilon}H\big(\varepsilon g(x) - y\big) + \frac{1}{\varepsilon}H(-y)\right|^2 \\
&= \frac{1}{2\varepsilon}\left(\int_{T^n}\frac{1}{2}\left|\big(u_\varepsilon(\cdot, \varepsilon) - u_\varepsilon(\cdot, -\varepsilon)\big) - g\right|\right)^2. \qquad (28)
\end{aligned}$$

Jensen's inequality was used to obtain (27). In (28), $u_\varepsilon(\cdot, y)$ denotes the trace of u_ε on $(\cdot, y)$. The equality holds, because u_ε is in H^1, and thus admits a representative that is absolutely continuous on a.e. line [12]. This energy cannot be bounded, unless $u_\varepsilon(\cdot, \varepsilon^\alpha) - u_\varepsilon(\cdot, -\varepsilon^\alpha)$ converges to g in L^1, and thus the jump of u across $\{y = 0\}$ equals g, since weak convergence in H^1 implies weak convergence of the trace.

(iii) We first assume that the trace of u at $y = 0$ from below, denoted by $T^- u$, is in H^1. Take

$$u_\varepsilon(x, y) = \begin{cases} u(x, y + \varepsilon) & \text{for } y \leqslant -\varepsilon, \\ T^- u(x) + \frac{y}{\varepsilon} H\big(\varepsilon g(x) - y\big) & \text{for } -\varepsilon < y < \varepsilon, \\ u(x, y - \varepsilon) & \text{for } y \geqslant \varepsilon. \end{cases} \tag{29}$$

Note that this function is in $H^1_{\mathrm{loc}}(\Omega)$, since the traces at $\pm\varepsilon$ match, inside the strip the y-derivative of u_ε is bounded by $\frac{1}{\varepsilon}$, and the x-derivatives of u_ε are bounded by the sum of the x-gradient of $T^- u$ and the x-gradient of g, both of which were assumed to be in L^2.
The elastic energy $\mathcal{F}_\varepsilon(u_\varepsilon)$ outside the strip of thickness ε remains exactly equal to $\mathcal{F}(u)$. The y-derivative of the function u_ε equals the n-component of $\xi_{\varepsilon g}$, and the x-derivative remains bounded by the (absolute) sum of that of $T^- u$ and that of g. Thus the integral over the vanishing domain $T^n \times (-\varepsilon, \varepsilon)$ goes to zero.
In order to obtain the result for arbitrary $u \in H^1_{\mathrm{loc}}$, one can employ the usual density argument. Functions with H^1-trace are dense and one can approximate with the energy bounded by $F(u)$.

□

The above theorem shows that for a nearly flat interface, the energy due to the shape of the phase boundary itself is equal to the energy of a function with a jump of the appropriate height g. It is well known [16], that the minimum attained at $\tilde{u}$ of this energy is equal to one half the $H^{1/2}$ seminorm squared of g, or,

$$\min_{\substack{u \in H^1(\mathbb{R}^\pm \times T^n) \\ [\![u]\!]_{y=0} = g}} \mathcal{F}(u) = \frac{1}{2}[g]^2_{H^{1/2}}. \tag{30}$$

REMARK 2.2 Note that we have not proved the Γ-convergence result for the case that g is only in $H^{1/2}$, since under this weaker assumption a recovery sequence can not be found. However, as we will see in Section 3, solutions of the evolution problem considered will have the required regularity.

2.4 *Approximation of the interaction energy*

We now turn to the scaled interaction energy

$$\mathcal{F}^\varepsilon_{\mathrm{int}} = -\int_{E \setminus \{y \leqslant y_0\}} (\nabla u_P - \xi_P) \cdot \xi_\Gamma \, \mathrm{d}x\mathrm{d}y + \int_{\{y \leqslant y_0\}} \left(\nabla u_P - \frac{1}{\varepsilon} \xi_{\varepsilon^{1/n} P} \right) \cdot \xi_\Gamma \, \mathrm{d}x\mathrm{d}y + \int_\Omega \frac{1}{2} \left\| \nabla u_P - \frac{1}{\varepsilon} \xi_{\varepsilon^{1/n} P} \right\|^2 \mathrm{d}x\mathrm{d}y \tag{31}$$

From the definition of u_P in (9) and (11), it is clear that as long as the interface is disjoint from the particles and does not cross them, $\nabla u_P - \frac{1}{\varepsilon} \xi_{\varepsilon^{1/n} P}$ is independent of the position of the interface and thus g. It follows then that the last two terms are independent of g under the assumption

above. Further, it follows that $\nabla u_P - \frac{1}{\varepsilon}\xi_{\varepsilon^{1/n}P} \to f(x,y)$ where f is independent of g under the assumption above. Therefore, we can write

$$\lim_{\varepsilon\to 0} \mathcal{F}^{\varepsilon}_{\text{int}} = \int_{T^n}\int_0^{g(x)} f(x,y)\,\mathrm{d}x\mathrm{d}y + C \tag{32}$$

for constant C under the assumptions above. Finally, when the interval crosses an interval, this form is still true with a redefined f.

2.5 *The approximate model*

The previous sections show that the energy of an interface described by the graph of a function g may be approximated as

$$\mathcal{E} = \frac{1}{2}[g]^2_{H^{1/2}} + \int_{T^n}\int_0^{g(x)} f(x,y)\,\mathrm{d}x\mathrm{d}y. \tag{33}$$

We postulate that the evolution of the interface is described as an L^2 gradient flow of g with respect to the energy. Since the variation of the $H^{1/2}$ seminorm yields the square root of the Laplacian, we obtain

$$g_t(x,t) = -(-\Delta)^{1/2} g(x,t) + f\big(x, g(x,t)\big). \tag{34}$$

This equation may be compactly written by its Fourier series,

$$\hat{g}_t(k,t) = -|k|\,\hat{g}(k,t) + \widehat{f\big(\cdot, g(\cdot,t)\big)}(k). \tag{35}$$

Note that the equation is still nonlinear, since the driving force f depends on g.

Finally, we assume that the distribution of precipitates is periodic in the direction of propagation of the interface. Thus, the forcing can be split up into a periodic *pinning potential* $\varphi(x, g(x))$ with zero average and a constant term F stemming from boundary conditions at $\pm\infty$, so that

$$f(x,y) = \varphi(x,y) + F. \tag{36}$$

This leads to the final model

$$g_t(x,t) = -(-\Delta)^{1/2} g(x,t) + \varphi\big(x, g(x,t)\big) + F \tag{37}$$

or

$$\hat{g}_t(k,t) = -|k|\,\hat{g}(k,t) + \widehat{\varphi(x, g(x,t)}(k) + \hat{F}. \tag{38}$$

for a given $\varphi : \mathbb{R}^{n+1} \to \mathbb{R}$ with zero mean.

Two comments are in order. First, it is open whether the Γ-convergence of the energy implies convergence of solutions to the gradient flow. Second, we assumed in approximating the interaction energy that the interface is disjoint from any of the precipitates. This is important for obtaining a local pinning potential. The pinning potential would be non-local in the absence of this assumption. An approximate model that accounts for this remains an open issue for the future.

3. Stick-slip behavior

In this section, we study the stationary equation

$$0 = -(-\Delta)^{1/2} g + \varphi + F \tag{39}$$

and the evolution equation

$$g_t = -(-\Delta)^{1/2} g + \varphi + F, \tag{40}$$

together with an initial condition, and denote them by $(39)_F$ and $(40)_F$, respectively, indicating the dependence on the behavior on the external force $F \geqslant 0$. Our strategy and results closely mirror those of Dirr and Yip [9] who considered the Laplacian case. In this section we will make the following assumption on the wiggly force $\varphi\colon T^n \times \mathbb{R} \to \mathbb{R}$.

HYPOTHESIS 3.1 The interaction force $\varphi(x, y)$ is periodic in y, i.e., $\varphi(x, y) = \varphi(x, y + 1)$, has vanishing average, i.e., $\int_{T^n \times [0,1)} \varphi(x, y) = 0$ and is Lipschitz continuous in both x and y.

3.1 *Solutions of the evolution equation*

In this section we collect some properties of solutions of the evolution problem $(40)_F$.

Proposition 3.2 *For any initial condition $g(\cdot, 0) = g_0 \in C^0$, the quasistatic evolution problem $(40)_F$ admits a unique global in time classical solution. Classical solutions to $(40)_F$ satisfy a comparison principle. Furthermore, for $g_0 \in L^2$, a mild solution to the evolution problem exists and is classical for any $t > 0$.*

Proof. We first note that the evolution equation $(40)_F$ can be cast in the form of [11], equation (2), by periodically extending φ to $\mathbb{R}^n$. Since in our model the function φ is assumed to be Lipschitz, it follows from [11], Theorem 5, that the problem admits a unique Lipschitz continuous viscosity solution, and thus satisfies a comparison principle. We further remark that the fractional Laplacian generates an analytic semigroup on the space of continuous functions on T^n (for a reference see for example [27], Chapter IX.11, and note that this property is well known for the 'regular' Laplacian), and thus the problem also admits a classical solution that can be found via a variation of constants-formula [24]. This also shows that the viscosity solution for the problem is periodic.

For an initial condition only in L^2, note that the fractional Laplacian also generates a semigroup on L^p, $p \geqslant 2$, with solutions in $H^{1,p}$, the domain of $-(-\Delta)^{1/2}$ for values in L^p. We thus can recursively find spaces of higher and higher integrability for our mild solution at positive time until we obtain a Sobolev-embedding into the space of continuous functions. □

The next proposition concerns an energy estimate of the solution to the evolution equation.

Proposition 3.3 (Energy estimate) *Fix $\tau > 0$. Then there exists a constant C depending only on f and τ, such that for any solution of $(40)_F$ we have*

$$\left[g(t)\right]_{H^{1/2}} \leqslant C e^{-t} \, ||g_0||_{L^2} + C \quad \text{for} \quad t > \tau. \tag{41}$$

Proof. First note that the mild solution of (40) is given by the variation of constants formula

$$\hat{g}(k, t) = e^{-kt} \hat{g}_0(k) + \int_0^t e^{-k(t-s)} \widehat{f\left(\cdot, g(\cdot, s)\right)}(k) \, \mathrm{d}s \tag{42}$$

for $k \in \{0, 1, 2, \dots\}$.

We have, for $t > 1$, by Plancherel's theorem,

$$\begin{aligned}
\big[g(t,k)\big]^2_{H^{1/2}} &= \sum_{k=1}^{\infty} k\,|\hat{g}(t,k)|^2 && (43)\\
&= \sum_{k=1}^{\infty} k\left|e^{-kt}\hat{g}_0(k) + \int_0^t e^{-k(t-s)}\widehat{f(\cdot,g(\cdot,s))}(k)\,\mathrm{d}s\right|^2 && (44)\\
&\leqslant \sum_{k=1}^{\infty} 2k\left|e^{-kt}\hat{g}_0(k)\right|^2 + \sum_{k=1}^{\infty} 2k\left|\int_0^{t-1} e^{-k(t-s)}\widehat{f\big(\cdot,g(\cdot,s)\big)}(k)\,\mathrm{d}s\right|^2 && (45)\\
&\quad + \sum_{k=1}^{\infty} 2k\left|\int_{t-1}^t e^{-k(t-s)}\widehat{f\big(\cdot,g(\cdot,s)\big)}(k)\,\mathrm{d}s\right|^2 && (46)\\
&\leqslant C_1 e^{-t}\,||g_0||_{L^2} + C && (47)\\
&\quad + \sum_{k=1}^{\infty} k\left|\sqrt{\int_{t-1}^t e^{-2k(t-s)}\,\mathrm{d}s}\sqrt{\int_{t-1}^t\left|\widehat{f\big(\cdot,g(\cdot,s)\big)}(k)\right|^2\mathrm{d}s}\right|^2 && (48)\\
&\leqslant C_1 e^{-t}\,||g_0||_{L^2} + C && (49)\\
&\quad + C'\sum_{k=1}^{\infty}\int_{t-1}^t\left|\widehat{f\big(\cdot,g(\cdot,s)\big)}(k)\right|^2\mathrm{d}s && (50)\\
&\leqslant C_1 e^{-t}\,||g_0||_{L^2} + C_2. && (51)
\end{aligned}$$

If $t \leqslant 1$, the integral from 0 to $t-1$ can be disregarded and the integral from $t-1$ to t runs from 0 to t, with no change in the estimates. In this calculation, we have used Hölder's inequality in (48) and the fact that $\int_{t-1}^t e^{-k(t-s)}\,\mathrm{d}s = \frac{1-e^{-k}}{k}$ thereafter. □

3.2 *Existence of pinned and space-time periodic solutions*

First we assert the existence of a stationary solution for zero external driving force.

Proposition 3.4 *Under Hypothesis 3.1, equation* $(39)_0$ *admits a weak solution in* $H^{1/2}$.

Proof. Note first that $H^{1/2}$ is compactly embedded in L^2, independent of dimension. One can thus find a minimizer of the energy

$$E(g) = \frac{1}{2}[g]^2_{H^{1/2}} - \int_{T^n}\int_0^{g(x)} \varphi(x,\gamma)\,\mathrm{d}\gamma\mathrm{d}x \tag{52}$$

among functions in $H^{1/2}_c = \{u \in H^{1/2} : \int_{T^n} u = c\}$ with average c. Now denote by

$$G(c) := \min_{g \in H^{1/2}_c} E(g) \tag{53}$$

the energy depending on the fixed average c. Since φ has zero average, we have $G(c+1) = G(c)$. Furthermore, G is Lipschitz by a simple comparison argument. Therefore, G admits a minimum for

some $c_0 \in \mathbb{R}$. The function g_{c_0} is a weak solution to $(39)_0$, since it minimizes the corresponding energy. □

Proposition 3.5 *Any weak solution to* $(39)_F$, $F \geqslant 0$ *is classical (and thus also a stationary viscosity solution).*

Proof. Plugging the weak solution g of the stationary equation into the variation of constants formula for the mild solution of the evolution problem, we find that g is a stationary mild solution, since

$$e^{-kt}\hat{g}(k) + \int_0^t e^{-k(t-s)}\widehat{f\left(\cdot, g(\cdot)\right)}(k)\,\mathrm{d}s = e^{-kt}\hat{g}(k) + \int_0^t e^{-k(t-s)}k\,\hat{g}(k)\mathrm{d}s = \hat{g}(k)$$

for $k \in \{0, 1, 2, \dots\}$. From the regularity properties of mild solutions with initial conditions in L^2, we find that the stationary solution must be classical. □

The following theorem asserts the existence of a threshold force, up to which – but not above which – a stationary solution exists.

Theorem 3.6 (Existence of a threshold force) *There exists* $F^* \geqslant 0$ *such that equation* $(39)_F$ *admits a solution for all* $F \leqslant F^*$*, while it has no solution for* $F > F^*$.

Proof. Consider

$$\Phi = \{F \geqslant 0 \text{ such that } (39)_F \text{ has a solution}\}.$$

Clearly, because of Proposition 3.4, $\Phi \neq \emptyset$. Also, if $F > \sup\varphi$, then $(39)_F$ has no solution. Define, therefore, $F^* = \sup\{\Phi\} < \infty$. Two things remain to be shown in order to establish the result:

(i) $F^* \in \Phi$.

(ii) There is a solution to $(39)_F$ for all $F < F^*$.

Proof of (i): Consider a sequence $F_j \nearrow F^*$ and corresponding solutions g_j of $(39)_{F_j}$ such that $0 \leqslant \int_{T^n} g_j \leqslant 1$. Such a sequence exists, otherwise F^* could not be the supremum of Φ. Since $\{F_n\}$ is bounded, we get uniform boundedness of $\{g_n\}$ in H^1 from a simple Fourier series argument. Therefore, there is a weakly converging subsequence (strongly in $H^{1/2}$) whose limit again satisfies $(39)_{F^*}$ in a weak sense.

Proof of (ii): Consider $0 < F < F^*$, and the solutions g^* and g_0 to the stationary equation with external driving force F^* and 0, respectively. By the periodicity of φ, and the continuity of the solutions we can assume $g^* > g_0$. These solutions are also super- and subsolutions to $(39)_F$, respectively. Therefore, there exists a solution to $(39)_F$. □

The next theorem proves the existence of a space-time periodic solution to $(40)_F$ above the critical force.

Theorem 3.7 (Existence of a space-time periodic solution) *For each* $F > F^*$*, there exists a unique* $0 < T(F) < \infty$ *and a unique function* $g(x,t)$ *satisfying* $(40)_F$ *such that*

$$g(x, t + T) = g(x, t) + 1. \tag{54}$$

Proof. Proposition 3.2 shows global existence of a classical solution. We will split the solution up into the evolution of the average and the evolution of the deviation of the average and use Schauder's fixed point theorem to prove the existence of a solution satisfying (54).

Define $p(t) = \fint g(x,t)\,\mathrm{d}x$ and $\xi(x,t) = g(x,t) - p(t)$. The functions p and ξ then satisfy

$$\dot{p}(t) = \fint f_g(x,t)\,\mathrm{d}x, \tag{55}$$

$$\hat{\xi}_t(k,t) = -k\hat{g}(k,t) + \widehat{f\big(\cdot, g(\cdot,t)\big)}(k) \quad \text{for } k \geqslant 1. \tag{56}$$

Consider the initial condition $\xi(x,0) = \xi_0(x) \in L^2$, and $p(0) = 0$. Since $F > F^*$, no stationary solution exists. Set thus $T(\xi_0) = \inf\{t > 0 : p(t) \geqslant p(0) + 1\}$. Note that there exists a constant τ, independent of ξ_0, such that $T(\xi_0) > \tau$. This follows from the fact that $|\dot{p}| \leqslant ||f||_{L^\infty}$. We also have $T(\xi_0) < \infty$ for all $\xi_0 \in L^2$, since otherwise one could find a stationary supersolution (and thus a stationary solution) to the problem at $F > F^*$, namely the pointwise limit for $t \to \infty$ of the solution to the evolution problem with initial condition ξ_0.

Now consider the nonlinear operator that advances the solution ξ in time, such that

$$\mathcal{T}(\xi_0) = \xi\big(\cdot, T(\xi_0)\big). \tag{57}$$

and we have

$$\hat{\xi}(k,T) = e^{-kT}\xi_0(k) + \int_0^T e^{-k(t-s)}\widehat{f\big(\cdot, g(\cdot,s)\big)}(k)\,\mathrm{d}s \quad k \geqslant 1. \tag{58}$$

From a similar calculation as in the proof of Proposition 3.3 it is clear that $||\mathcal{T}(\xi_0)||_{L^2} \leqslant e^{-\tau}||\xi_0||_{L^2} + C$, therefore, for $A = C/(1 - e^{-\tau})$, this operator maps the set $||\xi_0||_{L^2} < A$ onto itself. The regularity estimate in Proposition 3.3 also shows that $\xi(T)$ is bounded in $H^{1/2}$ independent of ξ_0, as long as $||\xi_0||_{L^2} < A$. The operator $\mathcal{T}$ is thus compact and an application of Schauder's fix point theorem yields the existence of a time-space periodic solution which is classical by Proposition 3.2. Uniqueness of T and g follow from the Proposition 3.8 below. □

Proposition 3.8 (Uniqueness of the space-time periodic solution) *The time-period T for a solution to $(40)_F$ satisfying*

$$g(x,t+T) = g(x,t) + 1 \tag{59}$$

is unique. Also, the solution itself is unique up to a time-shift so that, given two solutions g_1 and g_2 there exists t_0 such that $g_1(x,t) = g_2(x,t+t_0)$.

Proof. Assume that there exist two space-time periodic solutions g_1 and g_2, with time constants $0 < T_2 < T_1 < \infty$. Since the solutions are continuous and invariant under translations by an integer, one can find $N \in \mathbb{N}$ such that, for some time t_0, one has $g_1(\cdot,t_0) \leqslant g_2(\cdot,t_0) + N$. But since $T_2 < T_1$ there exists a time T after which the two solutions would have passed each other, contradicting the comparison principle.

Now, consider a solution G_1 with the initial condition $g_1(\cdot,t_0)$ and a solution G_2 with initial condition $g_2(\cdot,t_0)$. There have to exist a time T, an integer N, and a point x_0 such that we have

$$G_1(x_0,T) = G_2(x_0,t_0) + N \quad \text{and} \quad G_1(\cdot,T) \leqslant G_2(\cdot,t_0) + N, \tag{60}$$

i.e., the solutions have to touch at some time. Evolving both solutions in time from there on, one can see that they touch again after one time period. This, however, contradicts the strict comparison principle for classical solutions, unless $G_1(\cdot,T+t) = G_2(\cdot,t)$. □

4. Power laws near the depinning transition

In this section we investigate the effective interface velocity near the depinning transition. Specifically, we show that a range of behaviors are possible depending on the nature of the critical pinning point.

4.1 *One dimensional ordinary differential equation setting*

If φ depends only on the propagation direction, $\varphi(x, y) = \varphi(y)$, then we expect our solution g to be independent of x and satisfy the ordinary differential equation

$$\dot{g}(t) = \varphi\big(g(t)\big) + F \tag{61}$$

for a Lipschitz continuous, 1-periodic function $\varphi\colon \mathbb{R} \to \mathbb{R}$. This was studied earlier by Abeyaratne et al. [1] (also [5]). It is easy to see that the interface is stationary if

$$F \leqslant F^\star = -\min \varphi$$

and the effective velocity is

$$\bar{v} = \left(\int_0^1 \frac{\mathrm{d}g}{F + \varphi(g)} \right)^{-1} \tag{62}$$

for $F > F^\star$.

We now show through examples that a wide range of behaviors are possible near the depinning transition.

Example 1: Sharp minimum and logarithmic law. Let

$$\varphi(g) = 2\left| g - \frac{1}{2} \right| - 1,$$

for $g \in [0, 1]$ and extended periodically. Clearly $F^\star = 1$. A short calculation based on (62) shows

$$\bar{v} := \frac{1}{T} = \frac{1}{\log(F) - \log(F - F^\star)}$$

for $F > F^\star$. Thus,

$$\bar{v} \sim \frac{1}{-\log|F - F^\star|} \tag{63}$$

for F close to $F^\star = 1$.

Example 2: Power law. We now show that it is possible to obtain any power law $\bar{v} \sim |F - F^\star|^\beta$ for $\beta \in (0, 1)$ depending on the nature of $|F - F^\star|^\beta$ near the pinning points. Let $1 < \alpha < \infty$, $c_\alpha = 2^\alpha(\alpha + 1)$ and

$$\varphi(g) = c_\alpha \left| g - \frac{1}{2} \right|^\alpha - 1,$$

for $g \in [0,1]$ and extended periodically. Clearly $F^\star = 1$. So, for $F > F^\star$,

$$\bar{v} = \left(\int_0^1 \frac{dg}{c_\alpha \left| g - \frac{1}{2} \right|^\alpha + (F - F^\star)} \right)^{-1} = \frac{c_\alpha}{2} \left(\int_0^{1/2} \frac{dx}{x^\alpha + d^\alpha} \right)^{-1}$$

where $d = \left(\frac{F - F^\star}{c_\alpha} \right)^{1/\alpha}$. Now, since $x, d > 0$ and $\alpha > 1$,

$$(x+d)^\alpha \geqslant x^\alpha + d^\alpha \geqslant \frac{1}{2^\alpha} (x+d)^\alpha.$$

It follows,

$$\frac{c_\alpha}{2(\alpha-1)} \left(d^{-\alpha+1} - \left(\frac{1}{2} + d \right)^{-\alpha+1} \right)^{-1} \geqslant \bar{v} \geqslant \frac{c_\alpha}{2^{\alpha+1}(\alpha-1)} \left(d^{-\alpha+1} - \left(\frac{1}{2} + d \right)^{-\alpha+1} \right)^{-1}.$$

Therefore for $F - F^\star$ or d small, we conclude that

$$\bar{v} \sim |F - F^\star|^\beta \tag{64}$$

where $\beta = \frac{\alpha - 1}{\alpha} \in (0,1)$.

In particular, notice that for the smooth, but non-degenerate case of $\alpha = 2$, we obtain the square-root law $\bar{v} \sim |F - F^\star|^{1/2}$ for F near $F^\star$. This is an illustration of the result of [1] who showed that the square-root law holds whenever φ has isolated minima and the second-derivative is non-zero at the minima.

Example 3: Flat minimum and linear law. Let

$$\varphi(g) = \begin{cases} -4g & \text{for } 0 \leqslant g < 1/4, \\ -1 & \text{for } 1/4 \leqslant g < 3/4, \\ -1 + 4(g - 3/4) & \text{for } 3/4 \leqslant g < 1. \end{cases}$$

Again $F^\star = 1$ and a calculation based on (62) shows

$$\bar{v} = \frac{2(F-1)}{1 - \log(F) + F\log(F) + \log(F-1) - F\log(F-1)}$$

so that

$$\bar{v} = 2(F-1)$$

for F near $F^\star$.

In summary, a wide range of behavior is possible between the logarithmic and linear laws. Further, it is clear that the asymptotic behavior depends on the behavior of φ near its minima.

REMARK 4.1 It is not necessary to assume that φ is Lipshitz. (61) has a solution as long as $(\varphi + F)^{-1}$ is integrable. We can show that $F^\star = -\text{ess inf } \varphi$ and the asymptotic behavior near $F^\star$ depends on the the behavior of the Young measure near $F^\star$.

4.2 *Depinning in two dimensions*

In this section we study some examples numerically in two dimensions, and show that a wide range of behaviors are possible. Starting with an initial configuration $g(0) = 0$ and a fixed applied load F, we numerically integrate equation (35) using an explicit first-order Euler scheme. This explicit scheme is appropriate since a very small time step has to be chosen in order not to 'jump over' critically pinned states near the depinning transition. This immediately renders implicit schemes unnecessary. We also avoid using a higher-order scheme, since we want to sample the pinning force at short intervals for the numerical integration and not approximate it by a higher-order polynomial. The elastic force in our scheme, however, is calculated to high accuracy using discrete Fourier transforms. Once the interface has traveled a certain length on average (and never got stuck on the way), the final time is recorded. This way, a relation between the average velocity $\bar{v}$ and F is obtained. The interface is considered stuck if the L^2 norm of the driving force f drops below a certain threshold. This 'inner loop' is repeated with F chosen each time through a bisection algorithm, thus giving new upper and lower bounds for the critical F^* at each run. The program terminates after a certain accuracy for determining F^* has been reached. In Table 1 the standard parameters for the simulation can be found.

Example 4: Depinning behavior for smooth non-degenerate obstacles. The pinning potential φ used in this simulation is shown in Figure 3(a). It is smooth and contains isolated minima. To ensure smoothness, the pinning potential is described using a cubic B-spline (C^2). The constants used for this simulation are shown in Table 1. The evolution of the interface through one period is shown in Figure 3(b), where one can see that the interface spends most of its time near the critical stuck state depicted in Figure 3(c). In Figure 3(d), the relation between the average velocity and the force F is shown and compared to a square-root power law for F close to $F^\star$. The fit over almost seven decades is excellent.

For very high applied force one can see that the velocity turns toward a linear dependence on the applied force.

REMARK 4.2 As noted above, one obtains the square-root power-law ($\bar{v} \sim (F - F^\star)^{1/2}$ for $F > F^\star$, F near $F^\star$) for smooth pinning potentials in the one-dimensional ordinary differential equation setting. Dirr and Yip [9] showed that square-root power-law also holds for non-degenerate smooth pinning potential φ in the parabolic case (5) with the Laplace operator. Their proof relies solely on the comparison principle for critically pinned solutions, i.e., solutions u^* of the stationary equation

TABLE 1. Parameters used for the numerical examination of the depinning transition

Number of Fourier coefficients	1024
Length over which the interface velocity is averaged	4
Initial upper bound for F^* in bisection	0.5
Initial lower bound for F^* in bisection	0
Threshold for accuracy of F^*	$2 \cdot 10^{-9}$
Coefficient of elastic force	0.1
Time step	$1 \cdot 10^{-3}$
Threshold for stuck interface	$1 \cdot 10^{-14}$

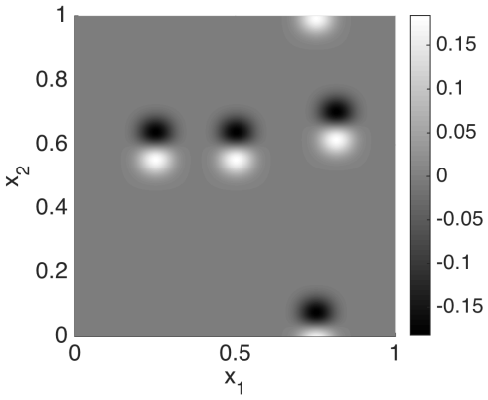

(a) Force distribution used to examine the general depinning behavior.

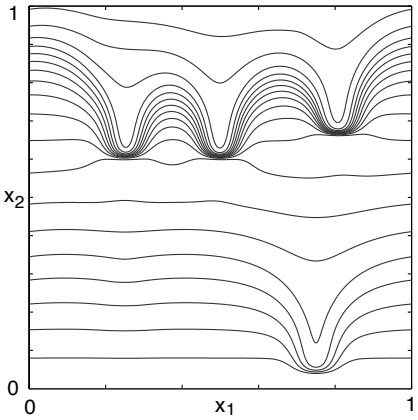

(b) The evolution of the interface through one period for $F = 0.04$. Snapshots were taken at equal time intervals, so one can see that the interface spends most of its time near the critical pinned state (see Figure 3(c))

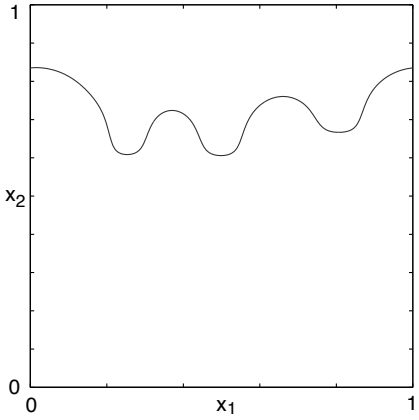

(c) Interface stuck at the inclusions for $F = 0.03$

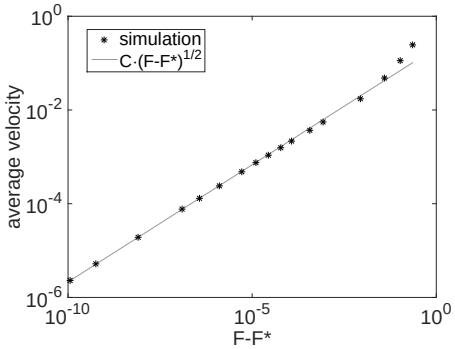

(d) Power law of the depinning transition

FIG. 3. The depinning behavior for smooth non-degenerate obstacles (Example 4)

(39)$_{F^*}$ at the critical force, and the spectral properties of the linearized operator

$$L_{u^*}v = -(-\Delta)^{1/2}v + f_u(x, u^*)v.$$

These properties as well as the comparison principle, however, remain unchanged even in our non-local equation 37. Therefore, the same result holds under the same non-degeneracy condition.

Example 5: Depinning behavior for smooth non-degenerate obstacles with different length-scales. We repeat the calculations in Example 4, but with pinning potential with five different characteristic

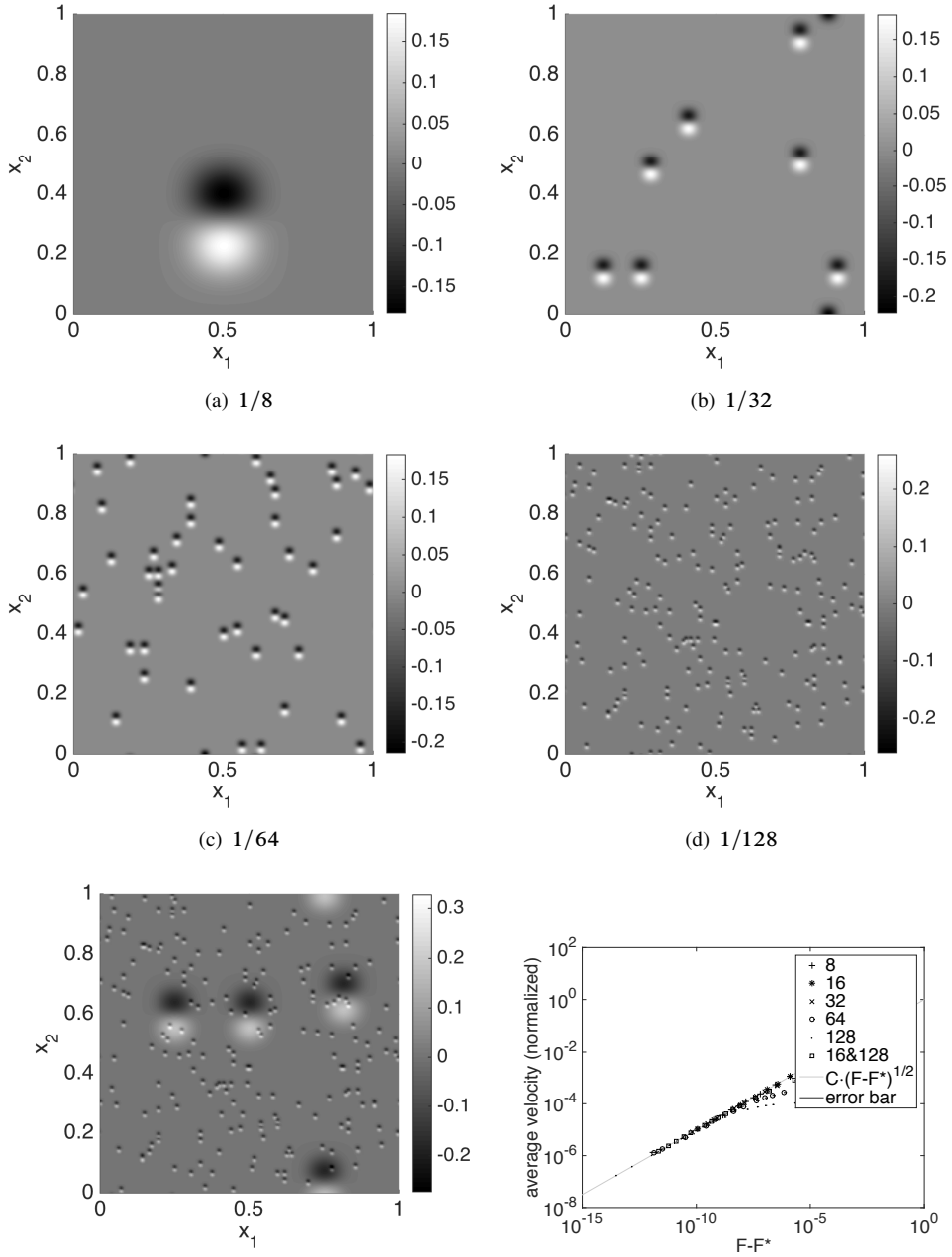

(a) $1/8$ (b) $1/32$

(c) $1/64$ (d) $1/128$

(e) $1/16$ and $1/128$ (f) Depinning Behavior

FIG. 4. The depinning behavior for smooth non-degenerate obstacles at various lengthscales (Example 5)

TABLE 2. The critical applied force for cases in Example 5

Size of pinning sites	Critical applied force F^*
1/8	0.0204
1/16	0.0307
1/32	0.0150
1/64	0.0143
1/128	0.0119

length-scales as shown in Figure 4. All parameters are kept as in Example 4 with the exception of the required accuracy for determining F^* (set to 10^{-15} here) and the threshold to consider an interface stuck (set to 10^{-17} here) for the simulation involving obstacles of size 1/128. We find square-power law in all these cases as shown in Figure 4(f). This figure also indicates the error bar in the calculation (visible only for the 1/64 case). The critical pinning force depends on case as shown in Table 2. We also consider a simulation with a pinning potential with two different length-scales as shown in Figure 4(e). We again obtain a square-root power law.

Example 6: Depinning behavior for sharp obstacles. We now consider a pinning potential with sharp minima as shown in Figure 5(a). To ensure a sharp minima, we use a bilinear interpolation on a square grid for the pinning potential. The obstacles are chosen to admit at their minima a piecewise affine shape in x_2-direction. All parameters are kept as in Experiment 1 except the accuracy for F^* and the "stuck threshold" which are set to 10^{-15} and 10^{-17}, respectively. The depinning behavior is shown in Figure 5(b) (again with error bars which are barely visible). The figure also shows the logarithmic law 63 predicted for the one-dimensional situation. We see that our results are consistent with this law.

Example 7: Depinning behavior for flat obstacles. We consider a pinning potential with flat minima as shown in Figure 5(c). In this simulation we again use cubic splines to construct the pinning potential. All parameters are kept as in Experiment 1. The depinning behavior is shown in Figure 5(d). We see that they follow a linear law predicted for the one-dimensional situation.

Example 8: Pinning asymmetry. Pinning is the result of interrogating the pinning potential using an elastic boundary. Therefore, it is non-local and depends on more than the local value of the pinning potential. Therefore, the same pinning potential φ can lead to a very different critical pinning force in the forward and the backward directions. This is illustrated in Figure 6. We consider the pinning potential illustrated in Figures 6(a) and its mirror image in Figure 6(c) corresponding to the forward and backward directions (positive and negative F). We find that the critical pinning force in the forward direction is $F = 0.046$, and that this is almost twice the the the critical pinning force in the forward direction of $F = 0.027$. Further, the stuck interface in the forward direction shown in Figure 6(b) is quite different from the mirror-image of the the stuck interface in the backward direction shown in Figure 6(d). Recently, Xia et al. [25, 26] have demonstrated this phenomenon in peeling of adhesive tape with patterned adhesive, a phenomenon also governed by our model (2).

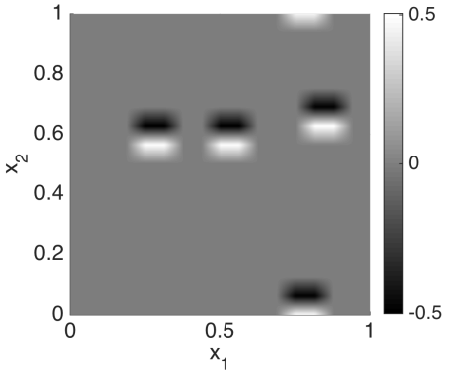

(a) Pinning potential for Example 6 (obstacles with sharp minima)

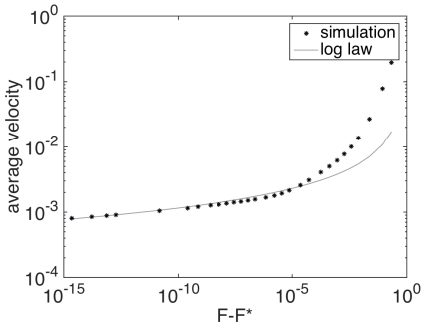

(b) Depinning behavior for Example 6

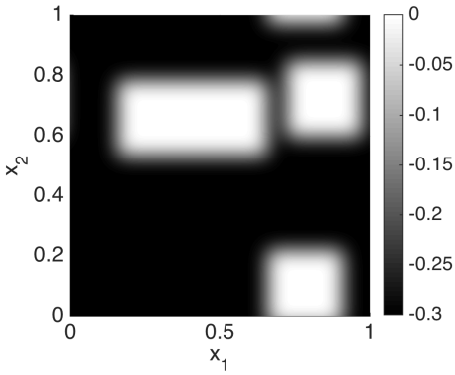

(c) Pinning potential for Example 7 (obstacles with flat minima)

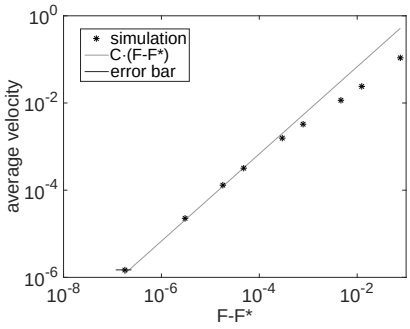

(d) Depinning behavior for Example 7

FIG. 5. Depinning behavior for pinning potential with sharp and flat minima (Examples 6 and 7 respectively). We obtain logarithmic behavior in the former and a linear law in the latter.

Acknowledgements. This work draws from the doctoral thesis of Patrick Dondl at the California Institute of Technology. It is a pleasure to acknowledge discussions with Bogdan Craciun, Nicolas Dirr and Aaron Yip. We gratefully acknowledge the financial support of the National Science Foundation (ACI-0204932, DMS-0311788, OISE-0967140).

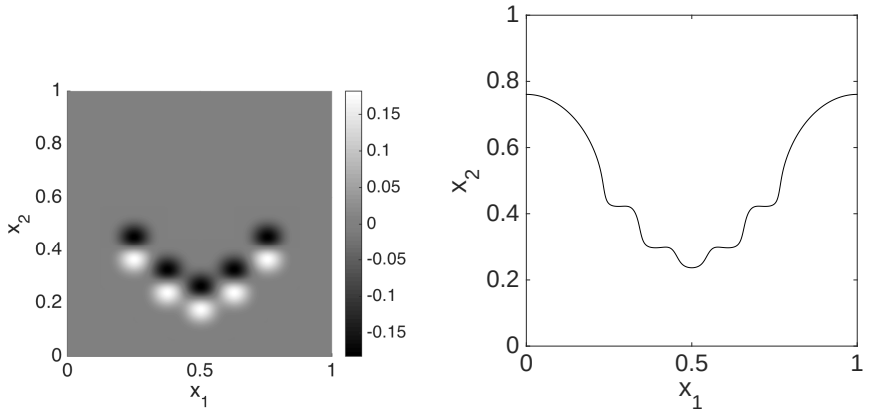

(a) Pinning potential for Example 8 in the forward direction

(b) Stuck interface near the depinning threshold for Example 8 in the forward direction

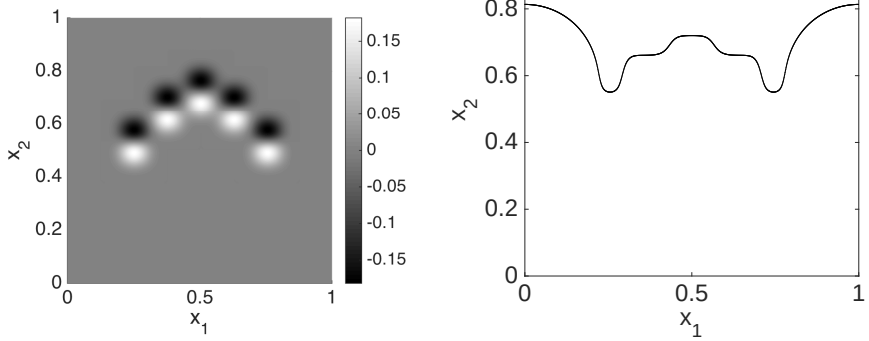

(c) Pinning potential for Example 8 in the backward direction

(d) Stuck interface near the depinning threshold Example 8 in the backward direction

FIG. 6. The forward and backward propagation with the same pinning potential can be quite different (Example 8)

References

1. Abeyaratne, R., Chu, C. & James, R. D., Kinetics of materials with wiggly energies: Theory and application to the evolution of twinning microstructures in a Cu-Al-Ni shape memory alloy. *Phil. Mag. A* **73** (1996), 457–498.
2. Abeyaratne, R. & Knowles, J. K., Implications of viscosity and strain-gradient effects for the kinetics of propagating phase boundaries in solids. *SIAM J. Appl. Math.* **51** (1991), 1205–1221. Zbl0764.73013 MR1127848
3. Abeyaratne, R. & Knowles, J. K., *Evolution of Phase Transitions: A Continuum Theory*. Cambridge University Press, 2006.
4. Barabási, A.-L. & Stanley, H. E., *Fractal Concepts in Surface Growth*. Cambridge University Press, 1995. Zbl0838.58023 MR1600794

5. Bhattacharya, K., Phase boundary propagation in a heterogeneous body. *R. Soc. Lond. Proc. Ser. A Math. Phys. Eng. Sci.* **455** (1999), 757–766. Zbl0990.74047 MR1700875
6. Craciun, B., *Phase boundary propagation in heterogeneous media*. PhD thesis, California Institute of Technology, 2001. MR2703191
7. Dirr, N., Dondl, P. W., Grimmett, G. R., Holroyd, A. E. & Scheutzow, M., Lipschitz percolation. *Electronic Communications in Probability* **15** (2010), 14–21. Zbl1193.60115
8. Dirr, N., Dondl, P. W. & Scheutzow, M., Pinning of interfaces in random media. *Inferfaces and Random Media* **13** (2011), 411–421. Zbl1231.35323 MR2846018
9. Dirr, N. & Yip, N. K., Pinning and de-pinning phenomena in front propagation in heterogeneous media. *Interfaces Free Bound.* **8** (2006), 79–109. Zbl1101.35074 MR2231253
10. Dondl, P. W., *Structure and evolution of martensitic phase boundaries*. PhD thesis, California Institute of Technology, 2007. MR3078547
11. Droniou, J. & Imbert, C., Fractal first-order partial differential equations. *Archive For Rational Mechanics And Analysis* **182** (2006), 299–331. Zbl1111.35144 MR2259335
12. Evans, L. C. & Gariepy, R. F., *Measure theory and fine properties of functions*. Studies in Advanced Mathematics. CRC Press, 1992. Zbl0804.28001 MR1158660
13. Forcadel, N., Imbert, C. & Monneau, R., Homogenization of some particle systems with two-body interactions and of the dislocation dynamics. *Discrete and Continuous Dynamical Systems. Series A* **23** 3 (2009), 785–826. Zbl1154.35306 MR2461827
14. Forcadel, N. & Monneau, R., Existence of solutions for a model describing the dynamics of junctions between dislocations. Zbl1181.35128 MR2491588
15. Gao, H. J. & Rice, J. R., A first-order perturbation analysis of crack trapping by arrays of obstacles. *Journal of Applied Mechanics* **56** (1989), 828–836. Zbl0729.73264
16. Garroni, A. & Müller, S., Γ-limit of a phase-field model of dislocations. *SIAM J. Math. Anal.* **36** (2005), 1943–1964 (electronic). Zbl1094.82008 MR2178227
17. Kohn, R. V., The relaxation of a double-well energy. *Contin. Mech. Thermodyn.* **3** (1991), 193–236. Zbl0825.73029 MR1122017
18. Koslowski, M., Cuitiño, A. M. & Ortiz, M., A phase-field theory of dislocation dynamics, strain hardening and hysteresis in ductile single crystals. *J. Mech. Phys. Solids* **50** (2002), 2597–2635. Zbl1094.74563 MR1935021
19. Mielke, A., Emergence of rate-independent dissipation from viscous systems with wiggly energies. *Contin. Mech. Thermodyn.* **24** (2012), 591–606. Zbl1258.74169 MR2992854
20. Mura, T., *Micromechanics of Defects in Solids*. Nijhoff Publishers, 1987. Zbl0652.73010
21. Ponson, L., Depinning transition in the failure of inhomogeneous brittle materials. *Phys. Rev. Lett.* **103** (2009), 055501.
22. Purohit, P. & Bhattacharya, K. Dynamics of strings made of phase-transforming materials. *J. Mech. Phys. Solids* **51** (2003), 393–424. Zbl1020.74020 MR1949580
23. Rice, J. R., 1st-order variation in elastic fields due to variation in location of a planar crack front. *Journal of Applied Mechanics-Transactions of the ASME* **52** 3 (1985), 571–579. Zbl0571.73104
24. Voigt, J., Regularity of mild solutions of nonlinear parabolic equations. *Transport Theory and Statistical Physics. An International Journal for Rapid Communication* **8** (1979), 17–22. Zbl0418.35057 MR0536455
25. Xia, S., Ponson, L., Ravichandran, G. & Bhattacharya, K., Toughening and asymmetry in peeling of heterogeneous adhesives. *Physical Review Letters* **108** (2012), 196101.
26. Xia, S. M., Ponson, L., Ravichandran, G. & Bhattacharya, K., Adhesion of Heterogeneous Thin Films II: Adhesive Heterogeneity. *J. Mech. Phys. Solids* **83** (2015), 88–103. MR3395882
27. Yosida, K., *Functional Analysis (Springer Classics in Mathematics)*. Springer, Apr. 1996.